J. Synchrotron Rad. (1997). **4**, 228–235

The Use of a Scanning X-ray Microprobe for Simultaneous XRF/XRD Studies of Fly-Ash Particles

Anders Rindby,[a] Per Engström[b] and Koen Janssens[c]

[a]Chalmers University of Technology/Göteborg University, Sweden, [b]ESRF, BP 220, F-38043 Grenoble CEDEX, France, and [c]University of Antwerp (UIA), Antwerp, Belgium. E-mail: f3bar@fy.chalmers.se

(Received 9 September 1996; accepted 8 January 1997)

With the opening of the first real 'third-generation' synchrotron source in Grenoble, in fall 1994, X-ray sources of unprecedented brilliances and qualities became available to the scientific community. Different X-ray analytical techniques could now be applied on a level that was unimaginable only a decade ago. Here are some preliminary results from an experiment where different analytical techniques have been applied on a micrometer level carried out at the most powerful synchrotron microbeam currently available in the world, the microfocus beamline (BL1) at ESRF. This beamline can now provide micrometer-sized X-ray beams with a flux density up to 10^{10} photons μm^{-2} at an energy of 13 keV and with a bandwidth of 10^{-4}. In this experiment, X-ray diffraction and X-ray fluorescence have been combined in order to obtain a precise and comprehensive micro-analytical description of micrometer-sized fly-ash particles. These types of particles are heavily inhomogeneous with a very irregular shape that makes them inaccessible to conventional micro-analysis. The experiment was performed in a scanning mode and two-dimensional images of different analytical information were reconstructed from the data recorded during the scan. The major features and limitations of this micro-analytical technique will be outlined and different examples on how the analytical information can be used for generating two-dimensional images of the sample will be demonstrated and discussed.

Keywords: microdiffraction; microfluorescence; capillary optics; fly-ash particles.

1. Introduction

A hundred years after the discovery of X-rays, the scientific and technical development of their different analytical applications is faster then ever. With the rise of the so-called 'third generation' of synchrotron sources, new possibilities for applying different types of X-ray analysis on a microscopic level have become available. As X-ray spectroscopy and diffraction can be carried out in open air with a relatively modest impact of neutral particles (photons), it does not require a vacuum, electrically or thermally conductive surfaces *etc.* Thus, X-ray analysis can be applied to samples that are normally inaccessible to conventional micro-analytical techniques (SEM, SIMS *etc.*) because of their thermal or conductive characteristics. Compared with electrons, X-rays have a much higher capability of penetrating the sample bulk, thus becoming less sensitive to surface layers and contaminants, which might have to be removed before performing any conventional analysis. In many cases, X-ray analysis can be performed without any preparation at all and is normally considered as a strictly non-destructive technique. As photoionization is the major interaction between X-rays and matter, in this energy region the sensitivity is high and sub-p.p.m. levels can be reached. This feature renders X-ray analysis as the 'technique of choice' in most cases where 'delicate' and precious samples are to be analyzed (lunar minerals, forensic material, archeological and art objects *etc.*). However, up to now X-ray analysis has been restricted to 'semi-micrometer' spatial resolution (100 μm or more) due to the limited brilliance of the available X-ray sources. With the rapid development of X-ray optics and the construction of dedicated synchrotron sources during recent years, the available flux density for micro X-ray analysis has increased by several orders of magnitude. In fall 1994 the first 'third-generation' synchrotron source, the ESRF in Grenoble, France, started to operate and X-ray flux densities far beyond any previous instrumentation became available to the X-ray community. With the combination of insertion devices such as undulators, focusing ellipsoidal mirrors and X-ray concentrators (capillary optics), it has been possible to achieve a flux density of $\sim 10^{10}$ X-ray photons μm^{-2} and still confined within a very small energy band of about only 1 eV. With such a flux density of highly monochromatic X-rays, both chemical (fluorescent X-rays) and structural (diffracted X-rays) information will become available. X-ray fluorescence spectroscopy will provide information on the concentrations of almost all chemical elements in the sample, all the way down to trace amounts, while the information contained in the diffracted radiation will reveal the stoichiometry of the major crystallographic components in the sample, the orientation and size of indi-

vidual crystals down to crystallites only a few nanometers in size. Only the very light elements (such as H, C, O) will be inaccessible for fluorescence analysis due to attenuation in air and detector windows.

All of this analytical information can be obtained on a microscopic level; however, much of this information would not make much sense if obtained at single points scattered over the sample surface. Thus, the X-ray beam has to be scanned in a regular way over a connective area of the sample surface.

The enormous amount of analytical data generated by such a scan cannot be handled in a conventional way and new algorithms and methods have to be developed and applied in order to obtain reasonable data reduction and to present relevant analytical information as two-dimensional images corresponding to the scanned sample area. For fluorescence data, many interesting developments are already occurring within the field of principal component analysis (Cross, Lamb, Ma & Paque, 1992) and other types of software post processing (Rindby & Voglis, 1992). However, for diffraction data the problem will become quite different as the data from each individual pixel in an image presents itself as an image.

2. Microdiffraction as an analytical tool

Microdiffraction has long been a very desirable analytical tool but inaccessible as a practical method for the analytical community due to the limited brilliance from conventional X-ray sources (like X-ray tubes) and efficient optical devices. However, microdiffraction has already been applied in the early 1950s when Amprino & Engström (1952) used a 30 μm beam for analyzing the crystallinity in bone tissues. However, they needed an exposure time of up to 48 h to obtain any significant result. Thus, real microdiffraction could not be applied until the introduction of high-flux micro-focused synchrotron sources in the 1980s. The first synchrotron set-ups used conventional optics such as the Kirkpatrik–Baez system, Wolter mirrors and ellipsoidal mirrors. However, none of these systems were able to generate microbeams well below 10 μm. Reviews on these early systems have been given by Jones & Gordon (1989), Rivers & Sutton (1991), Larsson & Engström (1991) and Rindby (1993).

The development of 'capillary optics' in the late 1980s has further improved the possibilities. Pioneering work on capillary-focused microdiffraction was performed by Yamamoto & Sakata (1989) and synchrotron-based microdiffraction by Dehaven & Goldsmith (1993). In 1994, Rindby, Engström & Voglis (1995) used microdiffraction for studying preferential orientations of crystallites in bone tissue samples. Diffraction from a submicrometer beam was recently demonstrated by Wang, Cargill & Noyan (1995).

Microdiffraction analysis has been applied with increasing interest as a means of analyzing not only crystallographic structures on a microscopic level but also crystallite size distribution and preferential orientations of assemblies of crystallites. For single-crystal analysis, a white (or at least a broad-band) beam is normally used. The crystallographic structure can then be determined from the Laue pattern in a conventional way. For the study of crystallites (nanometer-sized crystals), a monochromatic or narrow-band beam is preferential. If the crystals have dimensions much smaller than the beam size, a large number of crystals can be exposed at the same time. If these crystals (or crystallites) are randomly oriented, the total reflections from all the individual crystallites (of the same type) will form ring structures rather than localized spots on the recording device. If the number of exposed crystallites is 'small', the individual reflections might still be identified; however, if the number increases, a clear and continuous ring structure will appear (Lipson & Steeple, 1970).

When using microdiffraction as a micro-analytical method for highly inhomogeneous samples such as fly-ash particles, the problem is that we might have a mixture of both these types of analytical conditions as well as all intermediate stages. With the white-beam application, a single crystal can be identified from a large number of reflections; however, with the presence of a large number of crystallites any diffraction pattern would be drowned in an almost continuous ring structure, especially if we consider that the line broadening is substantial for nanometer-sized crystals. Thus, for these types of samples a highly monochromatic beam will be required.

3. Experiments and material

A combined microbeam XRD/XRF experiment has been performed on a microfocused synchrotron beamline (BL1 at ESRF) in order to test the analytical feasibility and to determine the sensitivity and accuracy of such a micro-analytical procedure. The experiment was carried out by a team of scientists from Chalmers University in Göteborg, Antwerp University, and the Central Research Institute of Physics in Budapest, at the ESRF in April 1995 in cooperation with the EDS group at ESRF.

The microfocused beamline at the ESRF has recently been equipped with a 2 μm focusing capillary or concentrator which, together with an ellipsoidal mirror, can provide a monochromatic beam with a flux density of $\sim 10^{10}$ photons μm^{-2} at a bandwidth of 10^{-4}.

The samples selected for the analysis were fly-ash particles collected at a lignite-fired power station in Japan. These particles consist of a mixture of small crystals of minerals (such as aluminium silicates) together with different types of precipitates and nanometer-sized crystallites. These types of particles are normally very difficult to analyze because of their highly inhomogeneous distribution of chemical elements, crystallinity and surface topology all related to the complexity of the process forming the particles. The fly-ash particles gain their complexity from both physical changes, such as melting, evaporation and condensation processes, and chemical changes, including thermal decomposition, oxidation processes and other intermediate reactions. The

final composition will be a mixture of primary minerals, such as quartz crystals, and secondary minerals and precipitates formed during the process of condensation. The average concentrations of different elements in the particles are basically a function of the primary coal minerals; however, the elemental distribution, crystallinity and other chemical characteristics are, to a large extent, a function of the thermodynamical conditions prevailing during the process of solidification.

The experiment was carried out by scanning the beam in a regular grid pattern over the fly-ash particles while recording the fluorescent intensities with an Si(Li) energy-dispersive X-ray detector and, at the same time, recording the diffraction pattern (in transmission mode) with a Photonics CCD X-ray camera. The beam was operated at an energy of 13 keV, which is suitable for diffraction patterns generated in a Laue transmission mode. At this energy the radiation power in the beam would be $\sim 2\,\mathrm{kW\,cm^{-2}}$ and the dose absorbed by the particles would be $\sim 10^{-8}\,\mathrm{J\,\mu m^{-3}}$, assuming normal attenuation. However, only a fraction of that energy will ultimately be converted into thermal energy. Still, these figures indicate that the sample would be subjected to a substantial temperature increase. However, from the study of the diffracted and fluorescent radiation during the exposure of individual pixels ($\sim 10\,\mathrm{s\,pixel^{-1}}$), there was no indication of any deterioration of the crystallographic structure or chemical composition within the sample.

From the diffraction and fluorescent intensities recorded, two-dimensional maps were constructed representing the distribution of specific minerals and trace elements in the fly-ash particles. Accuracy and sensitivity were determined from two different standard samples: a 'thick' sample of Orchard leaves (NIST SRM 1571) and a thin sample of glass (NIST SRM 1832). The sensitivity, in terms of p.p.m., was calculated from the thick sample and the sensitivity in terms of the minimum detectable amount was determined from the thin sample. A standard procedure was adopted where the minimum detectable signal was put equal to three times the square root of the background signal. Detection limits below 1 p.p.m. were reached for elements like Mn, Fe, Cu, Zn, Pb and As. For elements such as V, Mn, Co and Cu, minimum detectable amount values below 10^{-16} g were achieved.

The principle of the experimental set-up is shown in Fig. 1, while Fig. 2 shows a close-up of the capillary opening.

4. Generation of two-dimensional images from fluorescence and diffracted radiation

The principle of generating two-dimensional images of spectroscopic information from scanning devices has already been demonstrated by Dolby (1963) in the early 1960s. In general, any beam of particles can be used for analyzing the spatial distribution of any analytical parameter by just scanning the beam over the sample surface. The accuracy and quality of the analytical information will depend on the quality of the beam (flux density, time and space coherence *etc.*), the type of particles used (electrons, photons, heavy ions *etc.*) and the type of spectroscopy used to determine the analytical parameter in question. The spatial resolution will, in most practical cases, be directly dependent on the size of the beam itself. The luminosity in the images created from the scanning process is normally just the amplitude of the synchronized read-out from some recording device (*i.e.* electron detector in SEM) or the accumulated readout (during a specific time slice) within a certain spectroscopic region from some dispersive detector. In scanning X-ray analysis, two-dimensional images can be built up in very much the same straightforward way. An example of two-dimensional fluorescent maps is given in Fig. 3, which represents the distribution of zinc and arsenic over a cluster of fly-ash particles. The exposure time was $10\,\mathrm{s\,pixel^{-1}}$ and the step size was 2 μm.

Although the fluorescence intensity is related to the elemental abundance, the response of X-ray fluorescence from a point exposed to primary X-rays is almost never a simple function of elemental concentration since many other parameters have to be considered, such as depths distribution, sample surface topology *etc.* Some of these problems concerning quantification can be solved by looking at ratios or correlations between different elements (Rindby, Voglis & Attaelmanan, 1996). However, the relation between the recorded information and the final two-dimensional image is no longer a simple one. A typical example is given in Fig. 4, where the correlation graph between zinc and arsenic is presented together with a correlation map representing the spatial variation of the slope value of the correlation between the two elements. Each pixel in the correlation map corresponds to the slope value of the linear correlation between the nine pairs of points (the central pixel and the surrounding eight) from the two maps. Only those positions where these pairs of points generate a significant linear correlation with a correct intercept (see Rindby, Voglis & Attaelmanan, 1996) will be given a value within the grey scale of the image. Other points will just show up black. From the correlation map in Fig. 4, one can easily identify two connective areas, one inner and one outer area, on the lower particle, which means that the zinc/arsenic ratios are slightly different in these two areas. Note that the 'inner' region in the lower particle coincides very well with the distribution of the 'amorphous' material presented in Fig. 8. These findings indicate that at a certain stage in the process of solidification the inner and outer regions have been separated. For the upper particle the correlation between the two elements is not so strong and the slope value seems to vary in a more random way and no connective area is formed. The information obtained from such a correlation map concerns not only the different ratios of the two elements but also the depth distribution, which will affect the non-linear terms of the correlation graph.

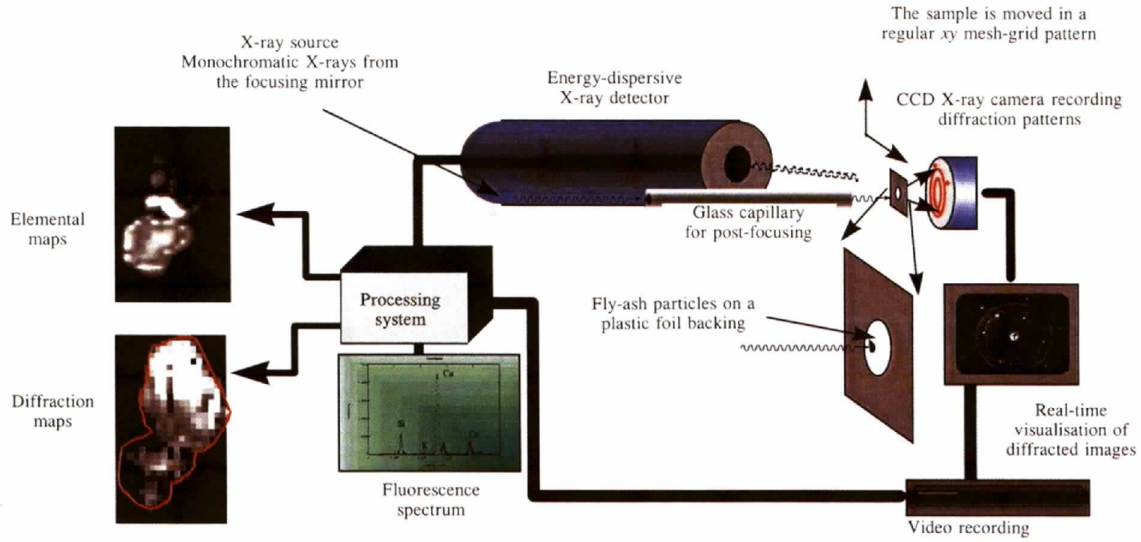

Figure 1
Principle of the experimental set-up.

For the diffracted radiation recorded from an X-ray microbeam scan, the problem is that the data recorded for each pixel itself is an image (rather than an analogue signal or a spectrum) where different chemical components are identified from complicated patterns of points or rings. The total amount of data from a diffraction pattern recorded at each point can correspond to several megabytes and has to be recorded within a few seconds. In Fig. 5, which shows a diffractogram recorded at the lower part of the fly-ash cluster, some of the general features in such a diffraction pattern are demonstrated. Simple image processing indicates that each pattern can consist of several hundreds of individual reflections superimposed on several systems of diffraction rings. Fig. 6 shows a selected data set of diffraction patterns from the entire scan over a fly-ash cluster. It is clear from this set of diffraction patterns that there is a large variation even between adjacent points, although the printed picture can never be of justice to the actual resolution in each individual diffraction pattern.

The simplest way to generate two-dimensional images is, of course, to just map up some well defined single reflection that can be attributed to some particular crystallographic system or mineral. Examples of such two-dimensional images are shown in Fig. 7, where the distribution of strong reflections from quartz crystals inside the fly-ash particles is demonstrated. As these crystals were much larger than the step size of the scanning beam, they can be followed from pixel to pixel and their position, extension and crystallographic orientation can be precisely determined.

Fig. 8 demonstrates the distribution of small crystallites of mullite and other types of precipitates or amorphous material which will appear as ring structures in the diffraction pattern. The mineral mullite is aluminium silicate mineral ($3Al_2O_32SiO_2$ or $2Al_2O_3SiO_2$) but does not appear naturally in coal mineral. It is formed from primary coal mineral as a result of the burning process itself. When formed it precipitates into small crystallites. In this case we have estimated the crystallite size to ~ 30 nm from the broadening of the reflections (Lipson & Steeple, 1970). The size of the crystallites formed is mainly a function of the rate of temperature variation during the process of condensation. Thus, the distribution and size of this mineral will give information on the thermodynamical conditions prevailing during the formation of the particle. Smaller crystals or even amorphous material will also give rise to a ring system; however, the broadening will make it difficult to identify these components. In Fig. 8(*b*) the distribution of such an amorphous material is shown.

5. Conclusions and discussion

It is quite clear that scanning X-ray microscopy can reveal microscopic information concerning the position, dis-

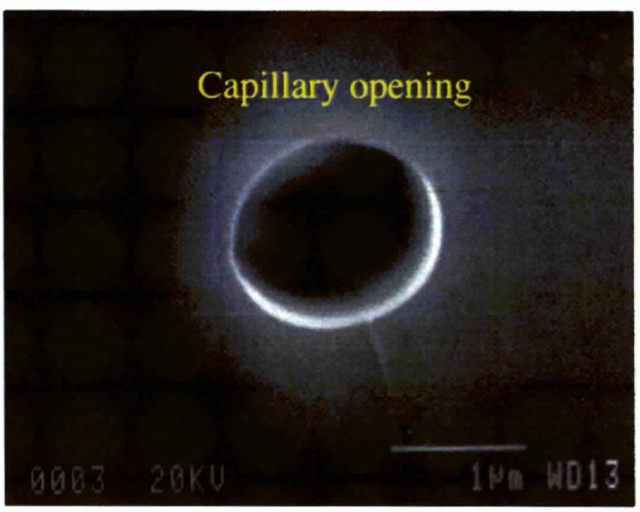

Figure 2
A close-up electron micrograph from the capillary opening used for the final focusing or 'concentrating' of the synchrotron beam. The samples are placed just in front of the capillary opening. The bar below corresponds to 1 µm.

tribution and orientation of 'large' single crystals down to nanometer-sized crystallites and at the same time the distribution of minor and trace elements, all in a quantitative and non-destructive way. This type of analytical information is normally not available from any conventional micro-analytical technique, especially not for samples which can be severely damaged by exposure to charged particle beams.

X-ray fluorescence analysis on different standard samples has shown that this microbeam set-up is capable of determining trace elements down to sub-p.p.m. levels and with a minimum detectable amount of less then 10^{-16} g. Thus, the technique can determine real trace-element distribution on a micro-scale. However, the calculated dose absorbed in the sample indicates that we are on the 'edge' of non-destructiveness.

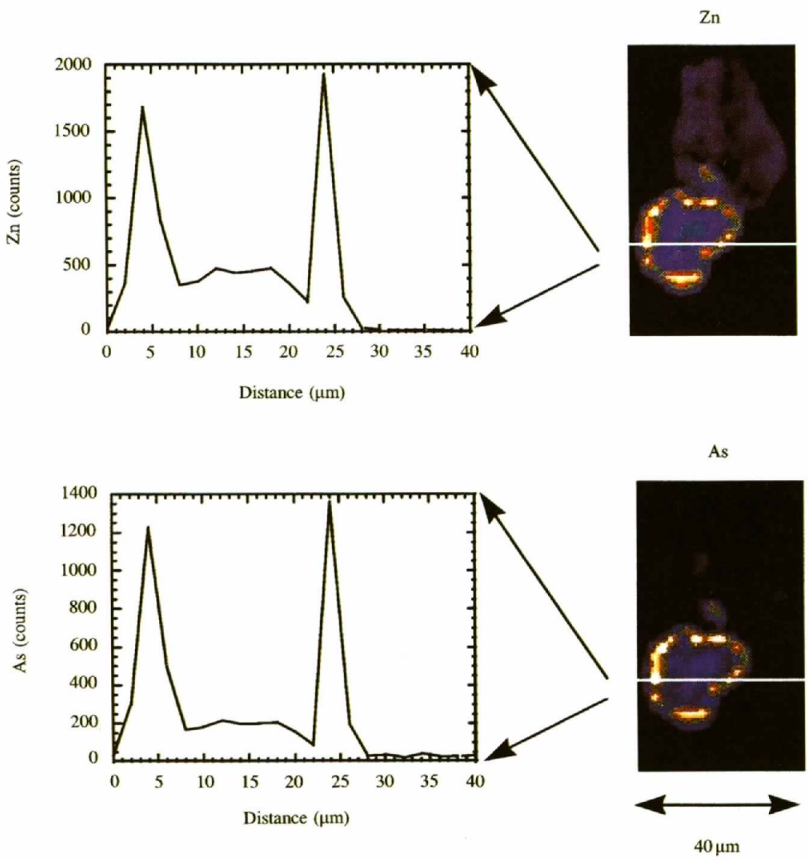

Figure 3
The elemental distribution of zinc and arsenic presented as 'temperature–colour' scale images (white/yellow indicates high fluorescence intensity and blue indicates low). The images have been smoothed. The intensity variation along the line across the lower particle is shown graphically. As can be seen from these two 'line scans', the variation of these two trace elements is almost identical.

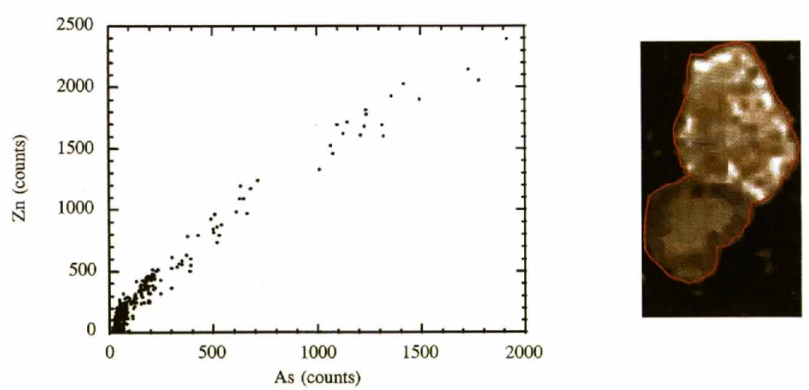

Figure 4
The correlation between zinc and arsenic is demonstrated both as a correlation graph (left) and as a correlation map (right). The graph indicates a strong and almost linear correlation between the two elements. In the correlation map the distinction between the two main particles in the cluster is quite clear. One can also easily identify two connective areas at the lower particle, indicating that the inner and outer part of that particle has been subjected to slightly different conditions during the process of solidification.

From the diffraction pattern we can easily establish the distribution of crystallographic components which appear in a well defined way in the diffractogram, like strong single reflections or rings. However, more comprehensive and sophisticated methods have to be developed in order to take full advantage of all the information stored in the diffraction patterns. The ability to determine the size distribution and preferential orientation of nanometer-sized crystallites on a micro-scale will enable us to understand more of the process of formation and thermodynamic 'history' of samples such as fly-ash particles or ancient remains from volcano break-out *etc.*

Cross correlation between diffraction and fluorescence data can provide interesting information about the circula-

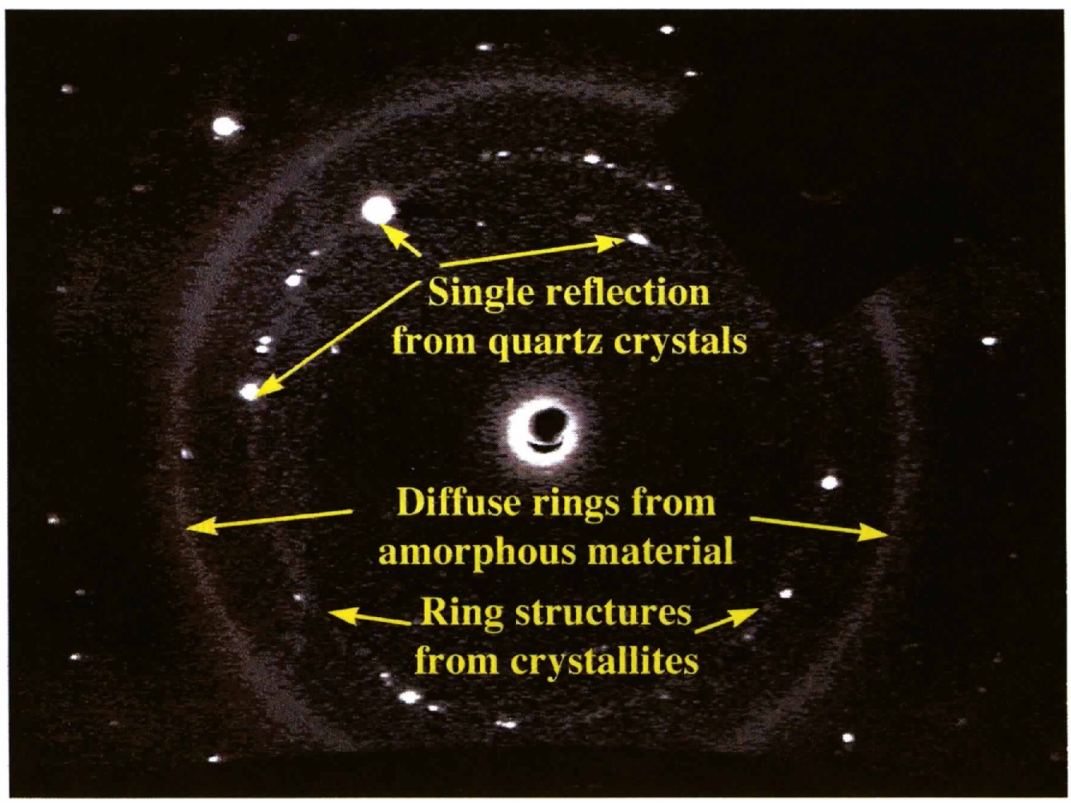

Figure 5
A diffraction pattern recorded from the lower part of the fly-ash particle cluster. The position, luminosity, peak shape *etc.* of all these different spots and rings appearing in the diffraction pattern contains information about crystallite size, orientation, local strain and lattice distortion.

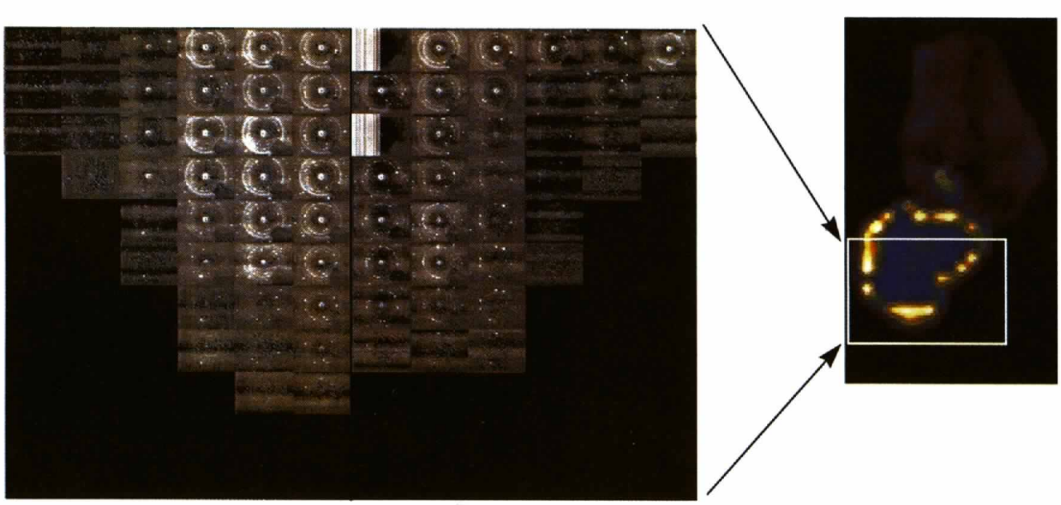

Figure 6
The complete data set of diffraction patterns from the bottom part of the lower particle. Note that although the original resolution has been drastically reduced, the spatial variation of the crystallographic structure can easily be observed.

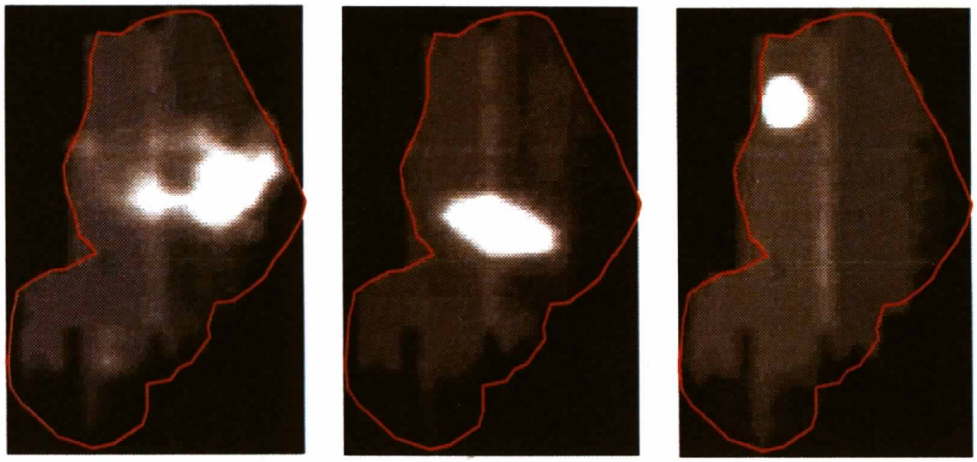

(a) (b) (c)

Figure 7
Single-crystal maps generated from (*a*) the 101 reflection in direction 2 o'clock, (*b*) the 101 reflection in direction 7 o'clock, and (*c*) the 102 reflection in direction 4 o'clock from quartz crystals inside the fly-ash cluster. The images have been smoothed.

tion and metabolism of heavy metals or other trace elements appearing in nature.

Still in the early 1980s, Ascenni and co-workers needed 24–48 h of exposure time to record diffraction patterns from bone tissues with a beam of 50–100 μm in diameter (Ascenzi, Bigi, Ripamonti & Roveri, 1983), while today we can observe similar diffraction patterns from a 2 μm beam 'live' on a video screen. This comparison corresponds to a difference in exposure time of about ten orders of magnitude, which indicates the tremendous development in X-ray science over the last two decades. However, we have not yet taken full advantage of these new analytical capabilities.

Other types of analytical X-ray methods, such as SAXS (small-angle X-ray scattering) or XANES (X-ray absorption near-edge spectroscopy), might also be applicable simultaneously with XRD and XRF and thus would give more detailed information of the microchemistry. Further developments in X-ray detector technology will allow for an even more efficient recording of the secondary X-rays generated by the primary beam, thus increasing the information content without increasing the energy load on the sample. The next generation of synchrotron sources will be able to generate even more powerful microbeams with improved characteristics and coherence. We are looking forward to that.

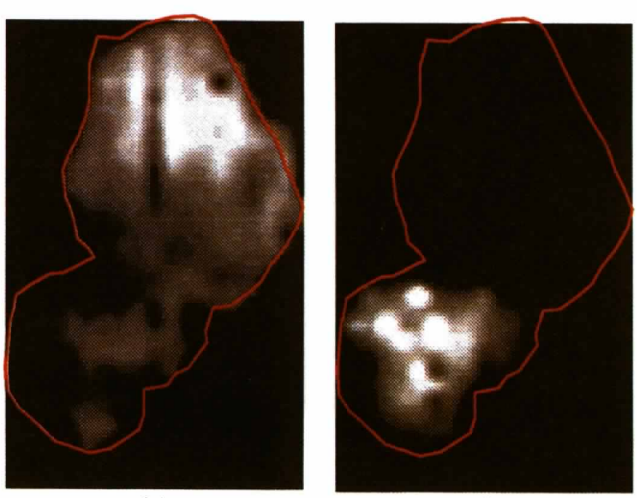

(a) (b)

Figure 8
Crystallite maps generated from the reflection rings (*a*) from mullite crystallites and (*b*) from a still unidentified amorphous material. The images have been smoothed.

We would like to thank Professor S. Török from CRIP in Budapest for her cooperation and for providing the fly-ash samples. We would also like to thank the ESRF beamtime committee for providing us the with beam time for this experiment. A special thanks to the staff of the BL1 beamline for the successful operation of the beam. This work has been partly financed by the Swedish Natural Science Council and the Belgian National Science Fund (Brussels).

References

Amprino, R. & Engström, A. (1952). *Acta Anat.* **15**, 1–22.
Ascenzi, A., Bigi, A., Ripamonti, A. & Roveri, N. (1983). *Calcif. Tissue Int.* **35**, 279–283.
Cross, B. J., Lamb, R. D., Ma, S. & Paque, J. M. (1992). *Adv. X-ray Anal.* **35**, 1255–1264.
Dehaven, P. & Goldsmith, C. (1993). *Mater. Res. Soc. Symp. Proc.* **309**, 275–279.
Dolby, R. M. (1963). *Proc. 3rd ICXOM*, pp. 483–493. New York: Academic Press.
Jones, K. W. & Gordon, B. M. (1989). *Anal. Chem.* **61**, 361A–366A.
Larsson, S. & Engström, P. (1991). *Adv. X-ray Anal.* **35**, 1019–1025.
Lipson, H. & Steeple, H. (1970). *Interpretation of X-ray Powder Diffraction Patterns.* London: MacMillan.
Rindby, A. (1993). *X-ray Spectrom.* **22**, 187–191.
Rindby, A., Engström, P. & Voglis, P. (1995). *Calcif. Tissue Int.* Submitted.
Rindby, A. & Voglis, P. (1992). *Adv. X-ray Anal.* **35**, 1247–1254.

Rindby, A., Voglis, P. & Attaelmanan, A. (1996). *X-ray Spectrom.* **25**, 39–49.
Rivers, M. L. & Sutton, S. R. (1991). *Synchrotron Rad. News*, **4**(2), 23–30.
Wang, P. C., Cargill, G. S. & Noyan, I. C. (1995). *MRS Symp. Proc.* **375**, 247–253.
Yamamoto, N. & Sakata, S. (1989). *Jpn. J. Appl. Phys.* **28**(11), L2065–2068.